JOURNAL OF PROPULSION AND POWER
Vol. 23, No. 4, July–August 2007

Rate-Based Model Predictive Control of Turbofan Engine Clearance

Jonathan A. DeCastro*
ASRC Aerospace Corporation, Cleveland, Ohio 44135

DOI: 10.2514/1.25846

An innovative model predictive control strategy is developed for a rapid-response, closed-loop active clearance control application, in which the objectives are to tightly regulate turbine blade tip clearances and also anticipate and avoid detrimental blade-shroud rub occurrences by optimally maintaining a predefined minimum clearance. At the heart of the controller is a rate-based linear parameter-varying model of a turbofan engine that extends performance to transient regimes in which conventional controllers begin to degrade. Engine-in-the-loop simulations of this rate-critical tip clearance control system with a variety of different actuators and uncertainty modes are presented, demonstrating the efficacy and versatility of this approach. Comparisons are made with a conventional linear quadratic control approach, where it is shown that substantial clearance gap reductions are possible by incorporating the strategy explored in this paper, thereby maximizing the cycle benefits that the tip clearance actuation/sensing hardware is capable of producing. Based on the results, it is concluded that the new strategy has promise for this and other nonlinear aerospace applications that place high importance on attaining strict control objectives during transient regimes.

Introduction

ALTHOUGH model predictive control (MPC) has been used for decades in some form or another in industrial processes, it is gaining ever more acceptance in aircraft propulsion applications due to advances in computing power of modern onboard control platforms [1,2]. Fast computation is necessary because the controller must generate current and future actuator commands based on open-loop receding horizon trajectories at each time instant [3]. The trajectory information allows the controller to optimize over the horizon while avoiding a predetermined set of constraints, such as saturation limits of an actuator or operational limits that define the safety margins of a particular plant or process. In specific propulsion applications such as aircraft engine control or active turbine tip clearance control, this control strategy offers a wide range of utility.

Figure 1 shows a general conceptual sketch of a new active clearance control system, where the actuated shroud is depicted as responding to changes in clearance measured by a clearance probe. It is envisaged that replacement of open-loop clearance control systems aboard modern aircraft engines (designed to achieve modest gains only at steady-state conditions such as cruise) with faster actively controlled systems will result in ultratight clearances in the high-pressure turbine, permitting lower emissions and higher fuel savings by decreasing thrust-specific fuel consumption (TSFC) as well as longer life through decreased exhaust gas temperatures (EGT) [4]. Specifically, every 0.01-in. reduction in clearance results in nearly 1% improvement in efficiency over all operating modes and 10°C reduction in peak EGT during transients [5]. The challenge in tip clearance control has always been to avoid any instance in which the turbine blades rub against the shroud and permanently damage the blade tips, which is most likely to occur as turbine components thermomechanically deform during engine or flight transients. Acceleration and deceleration engine events are the largest contributors to high-magnitude tip clearance variations, producing variations of 0.05 to 0.1 in. in less than 10 s [4]. In light of these challenges, it is essential that these new systems regulate the clearance gap as close as possible to the threshold at which full confidence for preventing blade rubs is obtainable. Certainly, advances in actuation and sensing hardware for active clearance control will allow for precise and rapid control of the shroud relative to the blades [6,7], but at these tight clearances, there are no guarantees that control will be rub free because there is no way of imposing mechanical limits to prevent the gap from becoming too small. With this new hardware operating in closed loop, even small control lags can significantly detract from the cycle benefits of tip clearance control. Therefore it is extremely advantageous to apply an MPC approach to guard against blade rubs and therefore enable operation with the tightest clearances that the hardware will allow.

Because MPC is heavily reliant on an open-loop plant model, it is important for the model to accurately describe the plant, in this case, a turbofan engine. In numerous cases, the pitfall in applying successful computationally intense model-based control strategies is in the complexity of the model, as is the case with nonlinear models with a high degree of parameterization (e.g., neural nets). On the other hand, lack of fidelity can result in poor performance or robustness. In this paper, a gain-scheduled, linear parameter-varying (LPV) MPC law is considered that has sufficient fidelity but minimal computational expense. In the past, gain scheduling has often been applied under the assumption that analytical models of the plant exist and are at the disposal of the control engineer, as in Heise and Maciejowski [8] and Shamma and Cloutier [9]. Unfortunately, because high-fidelity numerical engine models often used in gain scheduling applications are highly complex, it is nearly impossible to arrive at representative closed-form analytical models. A smaller group of papers, such as Mehra et al. [10], treat the use of Jacobian linearized LPV models for MPC, but the limitation of traditional LPV models is the loss of fidelity during transients, where near-equilibrium assumptions do not hold. In receding horizon control, modeling inaccuracies are especially troublesome because the recursive computation can propagate error and can even destabilize the system. To remedy these issues, the rate-based linearization method introduced by Leith and Leithead [11] is explored in this work, which is advantageous because it is conducive to rapidly varying plants. Using the same models and similar control structure as the Jacobian-based system, the performance of the MPC is enhanced for rate-critical control problems such as the tip clearance problem. This is the first known

Presented as Paper 5107 at the 42nd AIAA/ASME/SAE/ASEE Joint Propulsion Conference & Exhibit, Sacramento, California, 9–12 July 2006; received 15 June 2006; accepted for publication 23 February 2007.

*Research Associate, Controls and Dynamics Branch, NASA John H. Glenn Research Center at Lewis Field, 21000 Brookpark Road 77-1. Member AIAA.

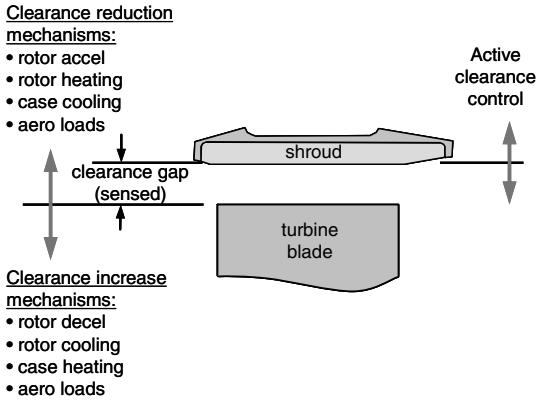

Fig. 1 Active turbine clearance control concept (cutaway view of turbine blade tip and shroud).

attempt at developing a rate-based LPV modeling technique (hereafter abbreviated as R-LPV) for MPC. The results of the assessment in this paper are useful as further guidelines from which to build MPC controllers for other aerospace applications (e.g., engine control), in addition to the application described here.

This paper is organized as follows. To lay the groundwork for the rate-based MPC, descriptions of both conventional and rate-based linearization methods for LPV models as they apply to numerical turbofan engine models are presented. Next, integration with the standard model predictive control problem setup is given, along with a simple technique to improve the computational expenditure of the rate-based internal model. Aspects of applying the MPC to a fast active clearance control device with tip clearance feedback are then described, and details of the actuators used and the high-fidelity engine model are given. Finally, results of active clearance control simulations are presented, demonstrating the comparative advantages of the proposed controller over the conventional approach. In that section, both servohydraulic and thermal deformation-based actuators are investigated to illustrate the versatility of this control approach.

LPV Models of the Turbofan Engine

Nonlinear systems, such as numerical turbofan engine models of the general form $\dot{x} = f(x, u, v)$, $y = g(x, u, v)$, can be expressed as LPV models to leverage linear control design theory and apply this theory in a piecewise manner. The LPV form is as follows:

$$\begin{aligned} \dot{x} &= A(\rho)x + B_1(\rho)u + B_2(\rho)v \\ y &= C(\rho)x + D_1(\rho)u + D_2(\rho)v \end{aligned} \tag{1}$$

The state vector, control input, disturbance input, and output vector are $x \in R^n$, $u \in R^{n_u}$, $v \in R^{n_v}$, and $y \in R^{n_y}$, respectively. The scheduling parameter vector is denoted by ρ and can be either exogenous, an input external to the plant, or endogenous, a state of the system. In the latter case, the system is said to be quasi-LPV.

Jacobian linearization [12] is often considered the standard method for extracting the system parameters as state-space matrices from nonlinear models, particularly input–output models that are defined numerically (i.e., "black box" models). Although it is possible in theory to linearize away from equilibrium, doing so is usually met with difficulty because the transient nature of the nonlinear system contaminates the perturbation decay characteristics needed for proper identification. As can be expected, linearized models valid only at steady-state operating points are problematic for maintaining strict gain-scheduled turbofan engine control performance through transients. When performed at various operating points, the resulting family of linearized models is referred to as a Jacobian LPV model:

$$\begin{aligned} \delta\dot{x} &= A(\rho)\delta x + B_1(\rho)\delta u + B_2(\rho)\delta v \\ \delta y &= C(\rho)\delta x + D_1(\rho)\delta u + D_2(\rho)\delta v \end{aligned} \tag{2}$$

The perturbation values $\delta x = x - x_0$, $\delta u = u - u_0$, $\delta v = v - v_0$, and $\delta y = y - y_0$ are functions of the steady-state equilibrium points, x_0, u_0, v_0, and y_0. Even if the steady-state operating envelope were fully populated (which is usually not the case), the result is by no means global because the state derivative equilibrium point $\dot{x}_0$ is assumed to remain zero everywhere. This implies that LPV trajectories are limited to a subset of actual trajectories of the nonlinear system exactly at equilibrium. This restriction is often relaxed by permitting transitions between points as long as variations in ρ are sufficiently slow, meaning that large-scale transient dynamics are assumed small compared to the equilibrium dynamics. As an alternative, Jacobian LPV models are sometimes supplemented with a nonlinear representation of the system to provide unmeasurable state derivatives necessary to compute $\dot{x}_0$ as the system undergoes transients. However, as pointed out by several authors, nonlinear engine models are computationally expensive and must be greatly simplified to operate adequately in real time [1,13]. Because of the enormous computational burden, nonlinear models are omitted altogether in quasi-LPV receding horizon control and thus the control does not account for state derivative equilibrium points [8,10]. As such, it should be made clear that the Jacobian LPV models referred to in the remainder of this paper do not correct for nonzero $\dot{x}_0$.

When applied in model-based control, the family of state-space models is scheduled by nearest neighbor selection, linear interpolation, or other more sophisticated methods. Because the LPV system in Eq. (2) is actually a nonlinear affine system, updates of the equilibrium points must be somehow supplied along with the system matrix updates, as depicted in Fig. 2. In the absence of a supplemental nonlinear model, the equilibrium values are often stored in the database alongside the Jacobians and scheduled the same. If system nonlinearities are particularly dominant, interpolation errors of these equilibrium values can appear as the trajectory progresses between operating points. Any receding horizon control method that uses a recursive quasi-LPV representation of the system can be negatively impacted by such errors as they propagate along the horizon, leading to control degradation and even destabilization.

As an alternative to Jacobian linearization, the LPV system in Eq. (2) can be transformed into a rate-based linear model, which is obtained by differentiation [11]. In this form, the perturbation quantities are no longer required to remain in the vicinity of the interpolation point, and thus the LPV states are identical to the actual system state derivatives. When differentiated, Eq. (2) takes on the following R-LPV form:

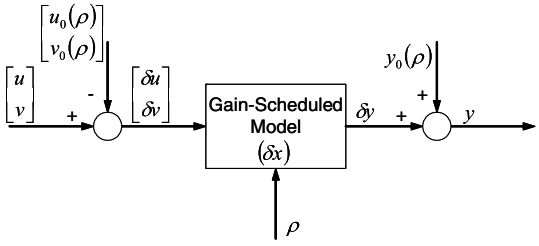

Fig. 2 Jacobian LPV models without correction for state derivative equilibrium point $\dot{x}_0$.

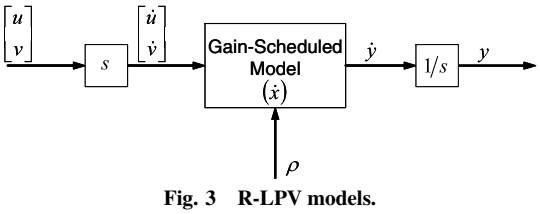

Fig. 3 R-LPV models.

$$\ddot{x} = A(\rho)\dot{x} + B_1(\rho)\dot{u} + B_2(\rho)\dot{v}$$
$$\dot{y} = C(\rho)\dot{x} + D_1(\rho)\dot{u} + D_2(\rho)\dot{v} \tag{3}$$

where the state vector is now represented by $\xi = [\dot{x}^T \quad y^T]^T$ and the state matrices are augmented appropriately. Figure 3 shows an input–output signal diagram for this model. The task of parameterizing Eq. (3) is identical to Eq. (2) because the perturbation states δx are first-order approximations to the derivatives of the actual states $\dot{x}$ in the limit sense. The fundamental advantage comes from the fact that the nonhomogeneous term that is present when Eq. (2) is expressed as a Taylor series expansion is assumed constant and disappears as a result of the differentiation. Because this term includes a linear combination of the model's equilibrium values, including $\dot{x}_0$, the model no longer requires $\dot{x}_0$ to remain zero. As a consequence, it is now possible for actual rates of change to be captured during faster transients, which may be viewed as an expansion of the valid operating bound encircling every linearization point and a relaxation in the speed at which ρ is allowed to vary. During slowly varying transients, Jacobian LPV models may be expected to experience errors that are a direct result of equilibrium point interpolation errors, while R-LPV models would tend to accumulate state errors brought about by interpolation of the Jacobians, because the Jacobians are still parameterized at equilibrium. Because both are susceptible to parametric interpolation errors, it cannot be assumed that the response of the R-LPV model will be any more accurate by assuming the nonhomogeneous term to be constant. Nevertheless, in the context of receding horizon control in gas turbines, R-LPV models lend themselves well to rate-critical control situations that call for avoiding operating limits typically encountered during transient operation, as in the tip clearance control application.

Because of the nature of the formulation, the R-LPV model suffers from several shortcomings which will now be addressed. First, the dimension of the state vector is now expanded to $n + n_y$, which may be computationally troublesome if the number of system outputs (measured or unmeasured) is exceptionally large. Second, due to the rate dependency of the controller structure, the measured disturbance inputs to the LPV models are brought in as a derivative, that is, $v' = \mathrm{d}v/\mathrm{d}t$. If the inputs to this derivative are susceptible to noise or biasing, especially in plants with high input–output sensitivities, this can amplify uncertainties with deleterious effects. In practice, however, this disturbance is often manifested as a demand-related event that is subject to little noise or other types of uncertainty. Moreover, estimation structures that operate upon separate disturbance states decouple the estimation loop from these effects. In the subsequent sections, these shortcomings will be addressed in the context of the tip clearance MPC application.

Model Predictive Controller in Rate-Based LPV Form

In this section, the practical problem setup for MPC is given. First, the disturbance model structure for output estimation in rate-based form is presented with treatment given to consolidating the estimator states with the expanded R-LPV states. Then, with this complete plant/estimator model, the R-LPV formulation of MPC is provided.

Disturbance Models in the Rate-Based Paradigm

In receding horizon control, input–output disturbance models are necessary to reduce the effects of any plant-model mismatch and to absorb exogenous disturbances affecting the plant but unknown to the model. It can be shown that all output channels will be free of steady-state error if the augmented system is detectable and the number of disturbance states equals the number of outputs [14]. To obtain asymptotic disturbance rejection, such models are often chosen to be pure integrators on each output channel. These integrators are normally appended to the model by expanding the state vector to incorporate the new disturbance states $d \in R^{n_y}$. However, in the R-LPV modeling approach, this would introduce undue computational complexity arising from incorporating additional n_y integrator states (a total of $2n_y$ more than the original model). Instead, the disturbance model integrators are borrowed from the R-LPV output integrators and their inputs are simply added to $\dot{y}$ in Fig. 3, transforming the state subvector y in Eq. (3) to $y + d$. The state-space equations are then

$$\dot{\xi} = \bar{A}\xi + \bar{B}_1 u' + \bar{B}_2 v' + \bar{B}_3 w_p \qquad y = \bar{C}\xi + w_m \tag{4}$$

with the augmented matrices

$$\bar{A} = \begin{bmatrix} A(\rho) & 0 \\ C(\rho) & \Lambda_{n_y} \end{bmatrix}, \qquad \bar{B}_1 = \begin{bmatrix} B_1(\rho) \\ D_1(\rho) \end{bmatrix}, \qquad \bar{B}_2 = \begin{bmatrix} B_2(\rho) \\ D_2(\rho) \end{bmatrix}$$
$$\bar{B}_3 = \begin{bmatrix} 0 \\ I_{n_y} \end{bmatrix}, \qquad \bar{C} = [0 \quad I_{n_y}]$$

As in Eq. (3), the augmented state vector ξ is composed of the state derivative vector and the output vector. Uncorrelated additive process and measurement noise intensities, $w_p \in R^{n_y}$ and $w_m \in R^{n_y}$, enter the disturbance model input channels and measurement channels, respectively. The diagonal filter matrix Λ_{n_y} is included to avoid pure integration at the outputs. Note that the R-LPV realization augmented with disturbance models will have the same number of augmented states as conventional LPV realizations with disturbance models.

Model Predictive Control Law

Given the R-LPV plant/estimator model, optimal control actions are found by minimization of a finite-horizon linear quadratic objective function with respect to the controls and the outputs [3]. Converting to discrete time, the linear quadratic cost function for the MPC law may be written as

$$J_k = \sum_{i=1}^{p} \Big[(y_{k+i} - y_{r,k+i})^T Q (y_{k+i} - y_{r,k+i}) + u_{k+i}^T R u_{k+i} \Big] \tag{5}$$

subject to the discretized version of the plant model of Eq. (4) and constraints on the manipulated controls and measured outputs at time k. The subscript r denotes the reference setting and p represents the prediction horizon. The symmetric, positive–definite weight matrices Q and R are to-be-determined design parameters, and the usual requirement holds that the pairs $(\bar{A}, \bar{B}_1)$ and $(\bar{A}, Q^{1/2})$ are stabilizable. A Kalman filter state estimator is designed on the condition that $(\bar{C}, \bar{A})$ is detectable, assuming the process and measurement noise covariances W and V, defined by the intensities w_p and w_m, respectively. It is important to note here that, because the rate-based MPC outputs are the derivatives of the control inputs, the output vector must be augmented with those control inputs to impose any weighting or constraints on the actual controls.

The LPV MPC formulation is achieved by computing state prediction equations recursively at each time step. Using the same state-space notation from continuous time for the discrete-time system equations, the state predictions are computed by

$$\begin{bmatrix} \hat{\xi}_{k+1} \\ \vdots \\ \hat{\xi}_{k+p} \end{bmatrix} = \mathbf{A}\hat{\xi}_k + \mathbf{B}_1 u'_{k-1} + \mathbf{B}_1^{\Delta} \begin{bmatrix} \Delta u'_k \\ \vdots \\ \Delta u'_{k+p} \end{bmatrix} + \mathbf{B}_2 \begin{bmatrix} v'_k \\ \vdots \\ v'_{k+p-1} \end{bmatrix} \tag{6}$$

where $\hat{\xi}_k$ are the estimated R-LPV states. The prediction matrices are

$$\mathbf{A} = \begin{bmatrix} \bar{A}(k) \\ \vdots \\ \prod_{i=0}^{p} \bar{A}(k+i) \end{bmatrix}, \qquad \mathbf{B}_1 = \begin{bmatrix} \bar{B}_1(k) \\ \vdots \\ \sum_{j=1}^{p-1} F_1(j, k+p) + \bar{B}_1(k+p-1) \end{bmatrix}$$

$$\mathbf{B}_1^{\Delta} = \begin{bmatrix} \bar{B}_1(k) & 0 & \cdots & 0 \\ \vdots & \vdots & \ddots & \cdots \\ \sum_{j=1}^{p-1} F_1(j, k+p) + \bar{B}_1(k+p-1) & \sum_{j=1}^{p-2} F_1(j, k+p) + \bar{B}_1(k+p-1) & \cdots & \bar{B}_1(k+p-1) \end{bmatrix}$$

$$\mathbf{B}_2 = \begin{bmatrix} \bar{B}_2(k) & 0 & \cdots & 0 \\ \vdots & \vdots & \ddots & \cdots \\ F_2(p-1, k+p) & F_2(p-2, k+p) & \cdots & F_2(1, k+p) \end{bmatrix}$$

where

$$F_*(j, \ell) = \left[\prod_{i=1}^{j} \bar{A}(\ell - i) \right] \bar{B}_*(\ell - j - 1)$$

In this representation, the control inputs are split into the present value of the control derivative u'_k and a vector of future control derivative moves.

The trajectory of predicted outputs is

$$\hat{y}_{k+i} = \bar{C}(k+i)\xi_{k+i} + D_2(k+i)v'_{k+i} \tag{7}$$

for each $i = 1, \ldots, p$. The dependence of the Jacobians on ρ is implied by their discrete-time dependence on k. From the above equations, it is readily apparent that the internal models assume quasi-LPV formulations (an internally computed scheduler) in forming the predictions, but may use an external scheduler for state estimation as long as state continuity between each realization is guaranteed. A fundamental requirement of the internal model is that it must be strictly proper, that is, zero gain at infinite frequency. For Jacobian LPV systems, this means formulating the plant model without the $D_1(k+i)$ term. In contrast, the fundamental model in R-LPV systems may be of any type because the R-LPV transformation is, by definition, one that maps any arbitrary system to a strictly proper system because the original D matrices become part of the $\bar{B}$ matrices. The rate-based paradigm thus provides more flexibility for the types of models that can be used.

Standard quadratic programming (QP) approaches are available to efficiently solve this convex constrained optimization problem; the approach employed here uses an "active set" method that optimizes on a subset of inequality constraints that are active at the current step. Common ways of making the control law computation more efficient are to limit the control horizon m to some $m < p$ or to update only intermittently (known as blocking). To expand the feasible set of the QP problem, the constraints are not posed as hard limits but instead are softened by incorporating a "slack variable" on the cost function that introduces an expensive penalty should any constraint violations occur. Computation is further streamlined by generating the Jacobians, estimator gains, and prediction matrices in an offline batch mode as a set of parsed arrays so that the on-line algorithm only needs to perform linear interpolation on these arrays at each time step.

Active Tip Clearance Control in a Commercial Turbofan Engine

As depicted in Fig. 1, the tip clearance control actuator is designed to move a segmented shroud structure toward and away from the turbine blades. The concept, as referred to in Lattime et al. [15], consists of several identical actuators that are placed at locations around the shroud circumference with each effecting movement in one shroud segment. It is assumed that each actuation point has a collocated clearance measurement at the shroud's frame of reference. In this configuration, the detected clearance is the difference between the combined deformation of turbine components (referred to as the unactuated clearance) and the actuator displacement, where a positive displacement results in smaller clearance. The active clearance control system can operate either upon a minimum detected clearance and single command signal, or upon several local clearance signals and actuator commands. The MPC is adaptable to both configurations, but only the single-output case is considered here.

Two actuator platforms were used to demonstrate predictive control behavior across different realistic hardware design scenarios: the first is a servohydraulic actuator and the second is a thermal deformation-based actuator. A detailed nonlinear model of the servohydraulic actuator described in DeCastro and Melcher [16] is implemented as the truth model and a parsimonious reduced order model is used in the MPC. The dynamics of the actuator are primarily driven by the servocontrol loop and are approximated here by the following third-order system with corner frequency of approximately 0.2 Hz:

$$G = \frac{1283}{(s + 223.2)(s + 4.035)(s + 1.424)} \tag{8}$$

The actuator stroke is measured by a transducer for servocontrol and is therefore assumed accessible to the engine control unit as a measured state of the system. The second actuator, a thermal-deformation based device, is similar to current thermal actuation systems that use secondary engine air to regulate the flange attachment to the shroud structure by way of a proportional air valve [4]. This device is represented by the first-order system

$$G = \frac{1}{\tau s + 1} \tag{9}$$

The difference between this actuator and current actuators is that the time constant τ is much faster, which may conceivably result from future modifications made to improve the heat transfer of these thermally activated systems. Because the intent of this case is purely illustrative, the thermal actuator internal model and truth model are taken to be identical. For both actuator types, constraints were placed on the minimum and maximum allowable control input settings, corresponding to zero and 0.1-in. displacements, respectively.

For this tip clearance application, a commercial engine simulation representative of a large, high-bypass turbofan engine coupled with either of the above actuator models was used as the truth model for closed-loop evaluation. The simulation features a detailed model of the turbine section component deflection to accurately represent demand-related clearance effects. On the basis that the MPC is to be implemented as an isolated control loop from the engine controller, a simplified closed-loop engine fan speed compensator was incorporated. The compensator is a linear, second-order system with a free integrator at the output, designed to obtain a slightly overdamped nominal closed-loop bandwidth of approximately 0.6 Hz. The requested fan speed is actually a mapping of the power

Table 1 Inputs and outputs for R-LPV tip clearance controller

Inputs	Outputs
Actuator command, *UACT*	Fan speed, *XN*2
Power lever angle, PLA	Fuel flow, *WF*
	Exhaust gas temperature, *T*5
	Stage 1 clearance, *CLR*
	Actuator position, *XACT*
	Actuator command, *UACT*

lever angle (PLA) and three environmental parameters (altitude, Mach number, and ambient temperature). Multimode controllers that typically deal with limits normally encountered with large transients have not been incorporated, but the MPC structure can be viably altered to accommodate this additional level of sophistication. Alternately, if the tip clearance MPC is implemented in a unified engine MPC (the most likely application), controller models are unnecessary because the MPC generates these engine commands.

A total of nine linear models of the closed-loop engine were generated at equispaced PLAs between ground idle and maximum power at sea-level static conditions, constructed with several sensed output channels and two input channels: delta clearance provided by the actuator and fuel flow (*WF*). Jacobians at these points were computed by perturbing these inputs, nine relevant engine states (fan and core shaft velocities and seven internal metal temperatures), and the three fan speed compensator states. The turbine component states are numerous and were omitted from the linearization. Because the operating conditions considered here are limited to constant altitude and airspeed, the scheduler is taken simply as the measured fan speed, *XN*2. With the hydraulic actuator model, the LPV model has a total of two inputs, 15 states, and six outputs; these I/Os are listed in Table 1. The total number of R-LPV internal model states is $n + n_y + n_u = 22$, only one state greater than the Jacobian LPV counterpart.

Figure 4 shows the interconnection of the rate-based active clearance control MPC and the turbofan engine plant outfitted with fast tip clearance actuators and feedback sensors. The exogenous disturbance δ_k is brought in only to the engine, while the demand-induced measured disturbance v_k is brought into both the engine and MPC. Here, v_k is simply PLA, but this may be extended to capture other sensed environmental inputs (ambient temperature, Mach number, altitude) if needed. To gain insight into the origin of the exogenous and demand-related disturbances acting on observable clearance, Table 2 presents the maximum magnitudes and bandwidths of disturbances that may be encountered during flight. Note that the demand-related effects are able to be anticipated by the predictive features of the controller.

Figure 4 also indicates the necessity to integrate the rate-based control variable u'_k and differentiate the measured disturbance signal v_k. As mentioned earlier, differentiation of input variables is necessary in the rate-based internal model framework, as depicted in Fig. 4. Such a transformation can amplify uncertainties if the inputs are imprecise or corrupted by noise, but because this application calls for a disturbance that is a function of throttle position, the signal is mostly free of noise and uncertainty. Nonetheless, examining the effect that these uncertainties have on transient performance is warranted to ensure that optimality is not compromised.

In this tip clearance implementation, minimization of TSFC and EGT is indirectly achieved by penalizing clearance excursions away

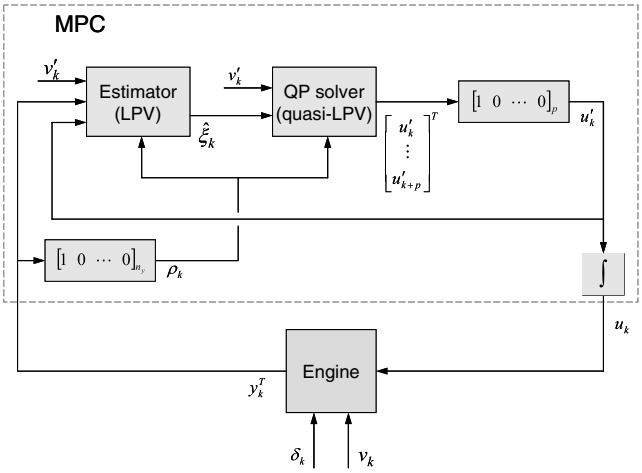

Fig. 4 Block diagram of MPC with R-LPV models. The first element of y_k corresponds to the scheduling variable (fan speed).

from a small-valued set point. The minimum clearance constraint and clearance set point are set to identical values to minimize clearance by maintaining this setting but avoid blade rubs at all costs by preventing excursions below it. The tuning procedure selected in this paper follows Doyle and Stein [18], where the objective is to first specify a desired loop transfer function (closed or open), then apply a quasi-deadbeat estimator to the loop to asymptotically achieve the specification. For all reported results, a 50-Hz sample rate is used and the ratio R/Q is set to 0.001.

In addition to the tip clearance control application, the theoretical groundwork may be applied to the turbofan engine control application as well. It should be cautioned that the tip clearance control problem differs from the engine control problem in that the MPC optimization problem remains mathematically convex with the quasi-LPV formulation in Eqs. (6) and (7) because tip clearance has little effect on the scheduling parameter, in contrast to fuel flow or other actuators. Although convexity is not guaranteed in the general case, it is still realistically possible for it to be preserved without exercising the use of mitigating techniques, such as sequential quadratic programming. Extension of quasi-LPV MPC to propulsion system control is not trivial and must be given special consideration.

Simulations

In this section, simulated results of the active clearance control MPC application are given and comparisons made between controllers derived using conventional internal modeling methods and the rate-based method explained in this paper. Additionally, ties are made to the practicality of this MPC implementation in active clearance control using the two tip clearance actuation methods described earlier.

Effect of Internal Model on MPC Tip Clearance Control

The rate-based MPC was compared with Jacobian MPC using the large-magnitude PLA transient shown in Fig. 5 with the control system outfitted with a servohydraulic tip clearance actuator. To properly compare the two MPC strategies when operating close to limits, it is helpful to break the MPC problem into its two basic

Table 2 Maximum magnitudes and bandwidths of various disturbances acting on measured clearance [4,17]

Disturbance	Source	Controllable	Magnitude	Bandwidth
Vibrations and unbalance	Exogenous	No	<0.005 in.	>100 Hz
Flight loads (thrust and maneuver)	Exogenous	Yes	0.02 in.	1 Hz
Centripetal loads and pressure differentials	Demand	Yes	0.04 in.	1 Hz
Thermal heat soak	Demand	Yes	0.02 in.	0.1 Hz
Gradual blade tip wear	Exogenous	Yes	0.03 in.	$\ll$ 0.1 Hz

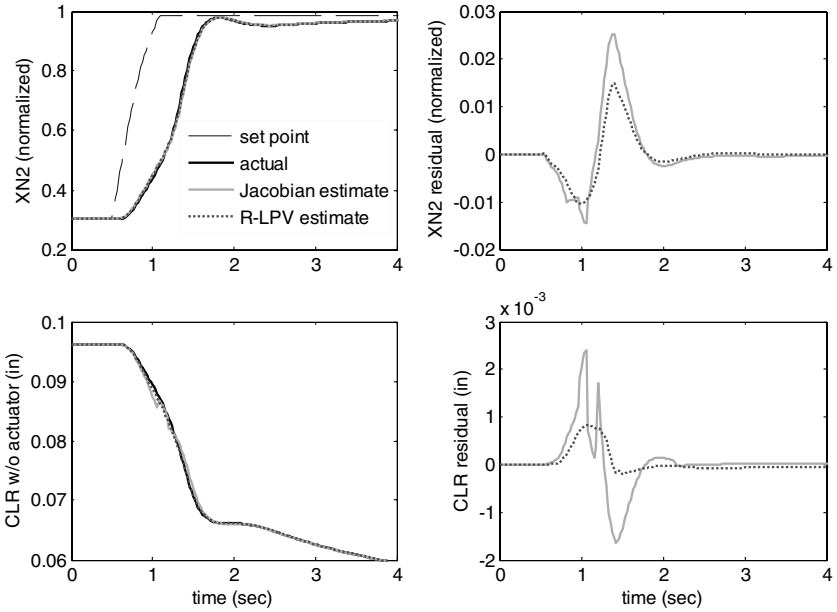

Fig. 5 Comparison between estimator performance for Jacobian and R-LPV models.

functions: estimation and prediction. The key component of the feedback control functionality of the MPC is the output estimator; if residual errors in state estimates are large when nearing a limit, then resulting tracking errors that result from inaccuracies in the computed states will increase the likelihood of exceeding the limit. Moreover, once the limit is exceeded, the controller will not effectively compensate for this violation. As shown in the time traces of actual and estimated variables in Fig. 5, the rate-based MPC maintains lower residual errors for the fan speed and clearance estimates over the entirety of the transient than the Jacobian MPC. Note that both estimators were designed with the same design parameters to achieve a deadbeat response. Although the unactuated clearance in the figure is not a physical output, it is included here because it represents the combined deformation of the turbine components and captures the evolution of clearance as a result of demand-related effects.

Because the cost function is based on the state estimates and state predictions, the predictive capabilities of the MPC have a large influence on the feedback gain. The predictions furthermore allow the MPC to operate much like a feedforward compensator when limit violations are anticipated, because the gain is adjusted in such a way to steer the plant away from the limit. To illustrate the effect of the state derivative equilibrium point $\dot{x}_0$ on the prediction accuracy, the state derivative for the $XN2$ state variable is shown in Fig. 6, along with snapshots of the model predictions for the input profile from Fig. 5. In Fig. 6, it can be observed that each of the Jacobian LPV predictions collapse onto a trajectory that deviates from the actual due to the lack of the $\dot{x}_0$ term. Although there is larger spread between R-LPV prediction curves at similar time instants, they tend to remain closer to the actual state derivative over a wide interval (at least 0.5 s). This is especially apparent at the time when the actual state derivative reaches its peak, 1.4 s. By noting the termination points of the R-LPV predictions, it is observed that the nonzero PLA derivative input causes the state derivatives to settle at nonzero values because this derivative is held constant throughout the horizon. Because of the problems that this can possibly pose for the controller, it is important not to lengthen the horizon to the point where these steady-state inconsistencies become influential in the response.

The time traces shown in Fig. 7 show a comparison between the closed-loop MPC responses using the two LPV models. To obtain an unconstrained clearance response that resembles the infinite-horizon response, the prediction horizon p was set to 20 samples and control horizon m was set to two samples. For the Jacobian-based controller in Fig. 7a, it is observed that the clearance oscillates and falls below the constraint (dashed lines) at about 1.3 s, violating the blade rub objective by about 1 mil. The prediction trajectory snapshots reveal that both the fan speed and unactuated clearance are incorrectly predicted and are especially poor between 1.3 and 1.5 s, corresponding roughly to the time when the constraint is violated. In Fig. 7b, it is revealed that the violation disappears with the R-LPV controller and the predictions in the top two traces more closely predict the initial rates. At 2.5 s, all internal model transients die out,

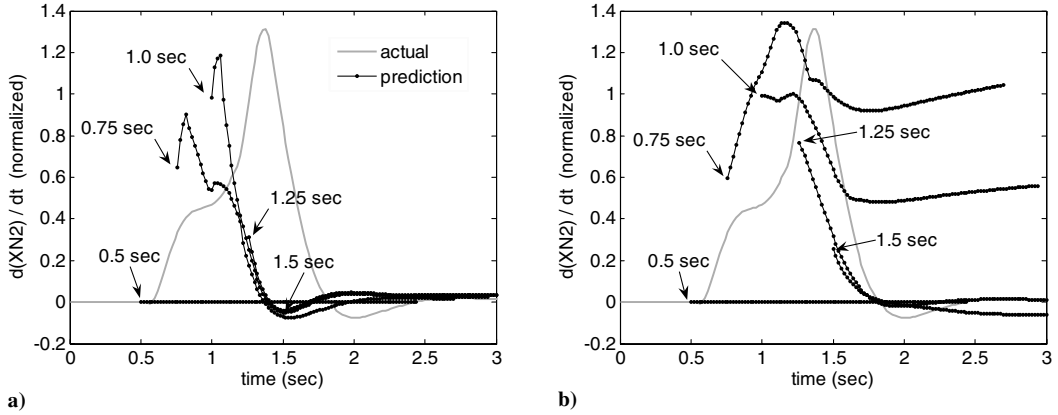

Fig. 6 Actual trajectory of fan speed state derivative with superimposed snapshots of prediction horizons. a) Jacobian LPV models and b) R-LPV models.

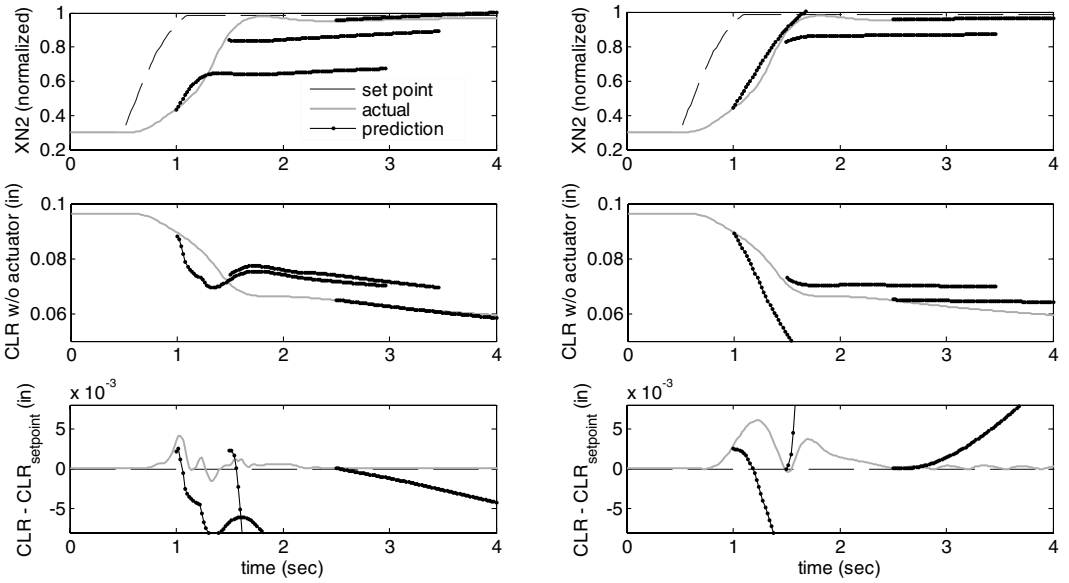

Fig. 7 Tip clearance control results with superimposed snapshots of prediction horizons. a) Jacobian LPV MPC and b) R-LPV MPC.

with any subsequent error being a result of the slow neglected dynamics. In the bottom trace of Fig. 7b, it can be noticed that the clearance predictions diverge more rapidly than their counterparts in Fig. 7a. This is because the rate-based MPC holds the derivative of the actuator command constant past the end of the control horizon, whereas, for conventional MPC, the actual command signal is held constant. Because the servohydraulic actuator is a velocity-controlled servosystem, clearance predictions show constant velocity in the Jacobian case and constant acceleration in the R-LPV case.

At this point, it is important to remark that these comparisons may be extended to MPC with a terminal cost [19] in place of sequentially computed predictions, which essentially removes the anticipative component and generates a pure feedback controller with constraints intact. Such a control strategy bears similarities to current model-based engine control systems, which may be a desirable option if the advantages of retaining predictive capabilities are outweighed by high computational complexity. There are two reasons why an R-LPV model-based controller is more conducive to rapid transients than with the Jacobian method. First, although computation of the feedback gain reduces to a simple gain schedule, it may be expected that the feedback gains in the R-LPV formulation will be more conducive to faster rates because ρ is now allowed to vary more rapidly. Second, as has already been established in Fig. 5, accuracy of the state estimates with the R-LPV controller will be greatly improved.

Flight Transient Assessment of the Rate-Based MPC

Whereas the previous evaluation was only concerned with using the feedforward attributes of the MPC in optimizing control actions based on demand-induced clearance events, actual in-flight situations require the need to reject exogenous disturbances in addition to the demand-related events, as outlined in Table 2. In the active clearance control application, clearance changes induced by flight loads acting on the engine are considered, whose effects become more problematic as clearance set points decrease because of the reduced margins against blade rubs. As alluded to in Olsson and Martin [17], there are multitudes of engine transients that occur during flight that are of interest in active clearance control, including takeoff, reburst, thrust reversal, hard turns, aircraft stall, etc. Each event contributes a demand-induced component on clearance due to PLA, etc., and a presumed unknown flight load-induced component as a result of turbulence, maneuvering of the aircraft, and asymmetric thrust loads that cause the engine to bend. Because of their large, rapidly acting contributions on clearance, the takeoff, thrust reversal, and aircraft stall events are employed to exercise the MPC laws given realistic clearance events that occur during normal operation; the magnitudes and rates of change of each event were reproduced approximately from actual flight data reported in [17]. Because takeoff and reburst have essentially an identical profile aside from the thermal state of the turbine at the start of the event, examining the transient MPC response with a takeoff event effectively serves the dual purpose.

The intent of this assessment is to compare the MPC strategy with a controller very similar to a linear quadratic regulator (LQG) control law to address the necessity of incorporating this constraint. The LQG formulation is accomplished by simply removing the clearance constraint from the MPC computations. Figure 8 shows the MPC response given the three event scenarios at nominal conditions for a thermal actuator with 1.6-s time constant ($\tau = 1.6$). This case represents an actuator whose response rate roughly matches the maximum deformation rate of the rotor during a power-increase event. To extend the anticipation capability, the prediction horizon p was increased to 50 samples and control horizon m to five samples. From the figure, the MPC response to a thrust reversal transient produces the most benefit over an unconstrained controller, eliminating the 2-mil excursion below the constraint. It is encouraging that enforcement of the clearance constraint is a result of very smooth actuator command signals rather than abrupt or highly oscillatory control actions. Although unconstrained responses in the remaining two events have milder constraint violations, the important observation is that the constrained controller satisfies the blade rub objective in both cases. One way of interpreting these results is to apply a "worst-case" analysis equally over all flight regimes. Using this reasoning, the clearance set point using this LQG controller must be 2 mils greater than the MPC set point to accommodate the possibility of the worst-case event and this would detract from exploiting the benefits of a tip clearance control system. Based upon a rule of thumb from past studies [5], the penalty on TSFC would be 0.2% over the entirety of the flight envelope and the penalty on EGT overshoot would be 2°C. To put these gains into perspective, it is reported in Lattime and Steinetz [4] that reductions of 15 mils are possible at steady state (yielding a 1.5% decrease in TSFC) by replacing state-of-the-art tip clearance control systems with generic, fast active systems.

Figure 9 shows the response with a thermal actuator with $\tau = 5.3$, a rate 60% slower than the previous case. This case is included to illustrate the consequences of applying MPC to an actuator that is slower than the rate of mechanical rotor growth, similar to state-of-the-art actuators. In the figure, the range of the control signal lies between one and zero and saturates beyond those values. For both

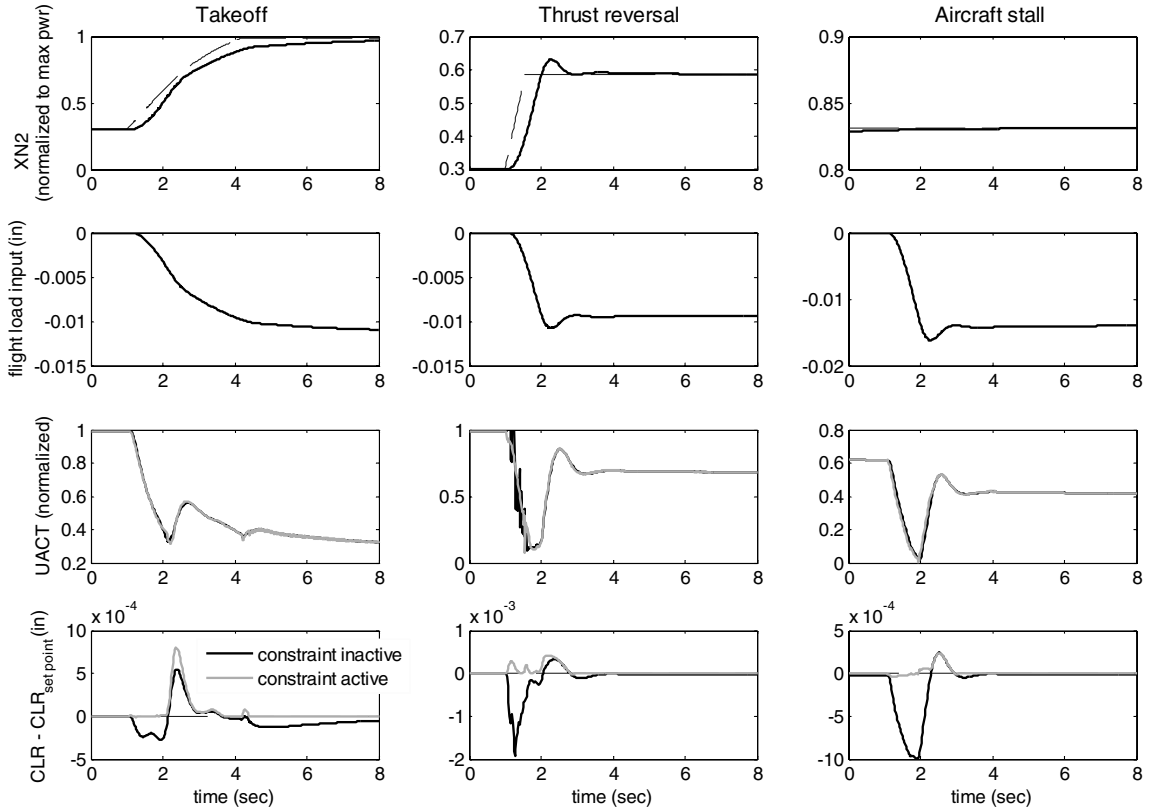

Fig. 8 R-LPV responses for fast thermal actuator.

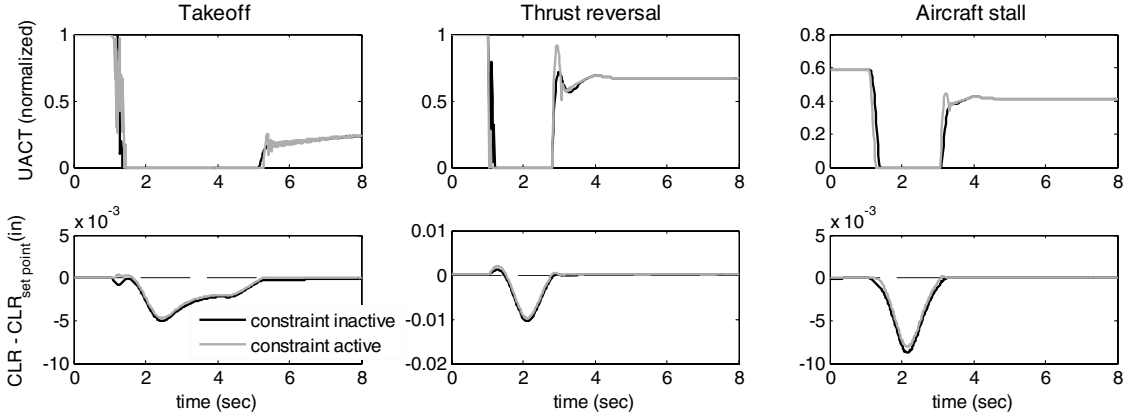

Fig. 9 R-LPV responses for slow thermal actuator.

controllers, the control signal saturates at zero in an attempt to move the shroud away from the blades. With the constrained controller, the combination of feedforward and feedback compensation of the event in the takeoff and thrust reverse events results in a slight increase in adjusted clearance before becoming altogether negative upon loss of authority. Although no anticipation is possible in the purely exogenous stall event, the adjusted clearance stays at zero longer than for the unconstrained case, a result of the more rapid compensation of the constrained MPC when riding the clearance constraint.

It may be noted in Fig. 8 that the exogenous aircraft stall event produces similar performance results to the other two cases. These results suggest that, for actuators with bandwidths well matched to the expected clearance rates of change, the predictive component could be removed and replaced with a terminal cost with little penalty. To the contrary, the results in Fig. 9 suggest that the MPC has room for further improvement for slower actuators. If it is possible to take advantage of any existing system delays (not captured here) between the PLA input and the engine controller, this would provide appreciable enhancements to the anticipative feedforward control element. Further gains may then be achieved by anticipation of the exogenous events, perhaps by direct estimation of the asymmetric flight load characteristics.

Table 3 summarizes the MPC benefits for the three actuators and also presents a case of tip clearance control amid off-nominal engine conditions. Comparing the fast thermal actuator with the nominal hydraulic device, both the unconstrained and constrained clearance values are quite different, which is directly related to suboptimality introduced with plant/model mismatch. Recall that the nonlinear hydraulic actuator is adopted as the truth model, while the thermal actuator only uses the linear model. With the exception of the slow thermal device, enforcement of the constraint results in commensurate amounts of clearance improvements for each. As echoed in Fig. 9, the MPC applied to the slow actuator offers some improvement, albeit less than a full-authority actuator does. The degraded engine case is implemented as a shift in engine parameters to roughly represent

Table 3 Minimum clearance for constrained and unconstrained R-LPV MPC. Values are in mils (1×10^{-3} in.)

	Unconstrained	Constrained	Delta
Thermal actuator, $\tau = 1.6$, nominal engine			
Takeoff	−0.28	−0.01	0.27
Thrust reverse	−1.93	−0.01	1.92
Aircraft stall	−1.00	−0.04	0.96
Thermal actuator, $\tau = 5.3$, nominal engine			
Takeoff	−5.01	−4.69	0.32
Thrust reverse	−10.5	−9.80	0.70
Aircraft stall	−8.71	−8.02	0.69
Hydraulic actuator, nominal engine			
Takeoff	−0.80	−0.18	0.62
Thrust reverse	−2.29	−0.50	1.79
Aircraft stall	−3.26	−0.71	2.55
Hydraulic actuator, off-nominal engine			
Takeoff	−0.60	−0.13	0.47
Thrust reverse	−2.15	−0.50	1.65
Aircraft stall	−3.26	−0.70	2.56

6000 cycles of engine service life degradation, as described in Sallee [20], coupled with a shift in fuel flow sensitivity of −5%. In a gross dynamical sense, any engine degradation is not expected to significantly impact the behavior of the engine, and much less the behavior of clearance dynamics. This important attribute is exemplified by the results.

To address the aforementioned issue concerning the integrity of the internal model amid uncertainties in the measured disturbance signal, simulation cases were generated where the PLA measured disturbance input was fouled by uncertainties. The results are shown in Fig. 10, where two cases show the effects of the MPC receiving PLA commands corrupted by a ±5% shift in sensitivity and a third where the PLA has additive white noise with variance of approximately 6% of full scale. The traces show that the introduction of noise causes excitation of higher-frequency controller modes, but no adverse effects in control performance. Although the controller sees a PLA derivative that differs greatly from the actual value entering the engine, the deadbeat estimator is quick to reject these disparities and the prediction is largely unaffected during the comparatively short span of the horizon. Naturally, longer horizons will exacerbate the effects of noise on the input channel, producing

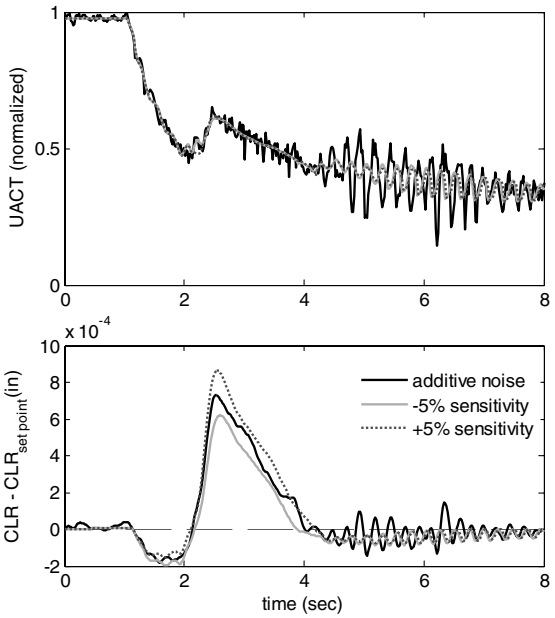

Fig. 10 Constrained R-LPV responses for a thrust reverse transient with corrupted measured disturbance.

an erratic or possibly divergent control signal. Although this evaluation is by no means comprehensive, the results indicate that R-LPV models are promising for use in MPC in the presence of these selected uncertainties.

Conclusions

In this paper, a new MPC strategy is applied to an active tip clearance control system, where it is critically important to maintain tight clearance gaps at all operating regimes but avoid violating a minimum clearance constraint that protects against detrimental turbine blade rubs. To accomplish this, an innovative MPC strategy is introduced to deal with the task of retaining these strict performance specifications during engine transients. With this technique, the standard LPV representation was transformed to rate-based form to extend the valid operating range to transient regimes, resulting in improved performance during power-increase events, where the control system is most susceptible to blade rubs. This rate-based form circumvents the need to parameterize standard LPV models away from equilibrium or with a full onboard nonlinear model of the turbofan engine operating in parallel, a procedure that is especially burdensome computationally when forming a quasi-LPV horizon. This new controller was compared in simulation against a standard gain-scheduled LQG controller, where it is shown that the clearance gap set point may be set to values 2 mils tighter than the LQG controller. In terms of cycle benefits, such a reduction improves TSFC by roughly 0.2% and EGT by roughly 2°C, a substantial improvement rewarded by prudent selection of an appropriate control law.

Acknowledgments

This work was supported by the Propulsion 21 program at NASA John H. Glenn Research Center at Lewis Field. The author gratefully acknowledges the insight and input provided by Kevin Melcher.

References

[1] Brunell, B. J., Bitmead, R. R., and Connolloy, A. J., "Nonlinear Model Predictive Control of an Aircraft Gas Turbine Engine," *Proceedings of the 41st IEEE Conference on Decision and Control*, IEEE, Piscataway, NJ, 2002, pp. 4649–4651.

[2] Fuller, J. W., Kumar, A., and Millar, R. C., "Adaptive Model Based Control of Aircraft Propulsion Systems: Status and Outlook for Naval Aviation Applications," ASME Paper GT2006-90241, May 2006.

[3] Maciejowski, J. M., *Predictive Control with Constraints*, Prentice-Hall, Harlow, England, 2002.

[4] Lattime, S. B., and Steinetz, B. M., "High-Pressure Turbine Clearance Control Systems: Current Practices and Future Directions," *Journal of Propulsion and Power*, Vol. 20, No. 2, 2004, pp. 302–311.

[5] Wiseman, M. W., and Guo, T.-H., "An Investigation of Life Extending Control Technologies for Gas Turbine Engines," *Proceedings of the American Control Conference*, IEEE, Piscataway, NJ, 2001, pp. 3706–3707.

[6] Geisheimer, J. L., Billington, S. A., Holst, T., and Burgess, D. W., "Performance Testing of a Microwave Tip Clearance Sensor," AIAA Paper 2005-3987, July 2005.

[7] DeCastro, J. A., Melcher, K. J., and Noebe, R. D., "System-Level Design of a Shape Memory Alloy Actuator for Active Clearance Control in the High-Pressure Turbine," AIAA Paper 2005-3988, July 2005.

[8] Heise, S. A., and Maciejowski, J. M., "Model Predictive Control of a Supermaneuverable Aircraft," AIAA Paper 96-3768, July 1996.

[9] Shamma, J. S., and Cloutier, J. R., "Gain-Scheduled Missile Autopilot Design Using Linear Parameter Varying Transformations," *Journal of Guidance, Control, and Dynamics*, Vol. 16, No. 2, 1993, pp. 256–263.

[10] Mehra, R. K., Prasanth, R. K., Bennett, R. L., Neckels, D., and Wasikowski, M., "Model Predictive Control Design for XV-15 Tilt Rotor Flight Control," AIAA Paper 2001-4331, Aug. 2001.

[11] Leith, D. J., and Leithead, W. E., "Input-Output Linearization by Velocity-Based Gain-Scheduling," *International Journal of Control*, Vol. 72, No. 3, 1999, pp. 229–246.

[12] Stengel, R. F., *Optimal Control and Estimation*, Dover, New York, 1994.

[13] van Essen, H. A., and de Lange, H. C., "Nonlinear Model Predictive

Control Experiments on a Laboratory Gas Turbine Installation," *Journal of Engineering for Gas Turbines and Power*, Vol. 123, April 2001, pp. 347–352.

[14] Pannocchia, G., and Rawlings, J. B., "Disturbance Models for Offset-Free Model-Predictive Control," *AIChE Journal*, Vol. 49, No. 2, 2003, pp. 426–437.

[15] Lattime, S. B., Steinetz, B. M., and Robbie, M. G., "Test Rig for Evaluating Active Turbine Blade Tip Clearance Control Concepts," *Journal of Propulsion and Power*, Vol. 21, No. 3, 2005, pp. 552–563.

[16] DeCastro, J. A., and Melcher, K. J., "A Study on the Requirements for Fast Active Turbine Tip Clearance Control Systems," NASA TM-2004-213121, July 2004.

[17] Olsson, W. J., and Martin, R. L., "B747/JT9D Flight Loads and Their Effect on Engine Running Clearance and Performance Deterioration; Nacelle Aerodynamic and Inertial Loads (NAIL)/ JT9D Jet Engine Diagnostics Programs," NASA CR-165573, Feb. 1982.

[18] Doyle, J. C., and Stein, G., "Robustness with Observers," *IEEE Transactions on Automatic Control*, Vol. AC-24, No. 4, 1979, pp. 607–611.

[19] Mayne, D. Q., Rawlings, J. B., Rao, C. V., and Scokaert, P. O. M., "Constrained Model Predictive Control: Stability and Optimality," *Automatica*, Vol. 36, No. 6, 2000, pp. 789–814.

[20] Sallee, G. P., "Performance Deterioration Based On Existing (Historical) Data; JT9D Jet Engine Diagnostics Program," NASA CR-135448, April 1978.

C. Tan
Associate Editor